AN EXPERIMENTAL INVESTIGATION OF PARTIAL CAVITATION ON A TWO - DIMENSIONAL HYDROFOIL

Jean-Baptiste Leroux, J. Andre Astolfi & Jean -Yves Billard
Institut de Recherche de l'Ecole Navale, 29240 Brest-Naval, FRANCE

Abstract

An investigation of leading edge partial cavitation was performed including the cavitation inception conditions, the cavitation patterns together with cavity length measurements. The investigation was enhanced by wall-pressure measurements using an instrumented hydrofoil equipped with seventeen wall-pressure transducers. Several experimental results are presented in the paper. A peak of pressure fluctuations was recorded at the cavity closure. The peak magnitude was seen to increase with the cavity length. For cavity lengths that did not exceed about half the foil chord, the peak originated from pressure fluctuations at a Strouhal number based on the cavity length close to 0.2. For longer cavities, the cavity began to pulsate at a lower frequency with the cavity length varying from the vicinity of the leading edge up to the trailing edge. The reason for such a phenomena is discussed.

1 Introduction

Leading edge attached partial cavitation is commonly encountered on a hydrofoil. It generally takes place at incidence angles for which a leading edge pressure peak occurs and is reduced below the liquid vapor pressure. Leading edge laminar flow separation has been shown to be a favorable condition under which attached sheet cavitation occurs, (Arakeri (1975), Franc & Michel (1985)). The interaction between the boundary layer and attached cavitation was also observed by Briançon-Marjollet, Franc & Michel (1985) and by Li & Ceccio (1996). In particular bubbles travelling in a laminar flow close to the foil surface were observed to produce locally a turbulent region and could temporarily sweep away a portion of attached cavitation at the foil midchord.
However, Zhang, Gopalan & Katz (1998) pointed out that it could also occur on surfaces without laminar separation (see also Astolfi *et al.* (2000) or Laberteaux & Ceccio (2001) which did not detect leading edge flow separation on hydrofoils). Local pressure distribution, local surface imperfection or micro-bubbles (which can induce a local flow separation) and surface nucleus could also be favorable conditions for sheet cavitation to occur. This is particularly relevant at full-scale flow for which transition is expected to occur and to remove flow separation (Huang & Peterson (1976), Huang (1986)). At the early phases of development, leading edge partial cavitation is steady ; consequently cavity length does not change significantly. The liquid-vapor interface is smooth and has a glossy aspect along a short distance from the leading edge. At the end of the cavity it breaks partially into small bubbles. As the cavity expands, the liquid-vapor interface become distorted, wavy and unstable yielding to breakup and unsteadiness. At this stage significant variations of the location of the cavity closure point are observed while shedding vapor structures called "cloud" cavitation. This process induces high-level pressure pulses (Le, Franc & Michel (1993)) and is known to be one of the most destructive forms of cavitation. The main cause of cavity destabilization on two - dimensional flows was often attributed to a reverse flow (re-entrant jet) formed at the end of the cavity (Kawanami, Kato & Yamaguchi (1998)). However, Callenaere, Franc & Michel (1999) provided evidence of a re-entrant jet only if the adverse pressure at the end of the cavity was sufficiently high and specially for relatively thick cavity ; for thin cavities no evidence of a re-entrant jet was observed in accordance with Zhang *et al.* (1998)'s observation. Laberteaux & Ceccio (2001) observed two types of partial cavities depending on the body studied : open cavity without (or very weak) re-entrant flow or unsteady re-entrant cavity on hydrofoils. From a numerical point of view, a large number of papers aimed at computing attached partial cavitation using various models, for instance Kubota, Kato & Yamaguchi (1992) using an unsteady bubble two-phase viscous flow model, or the paper by Kinnas & Fine (1993) using a potential-based boundary element method. Although some works have tried to compare experiments and numerical results in a common project (Brewer & Kinnas (1995), Pellone, Maître & Briançon-Marjollet (2000), Arndt, Song, Kjeldsen, He & Keller (2000)), it appears that modeling still requires

well-documented experimental data under highly controlled conditions. The flow near the cavity closure region requires closer examination. The paper deals with a careful experimental investigation of cavitation inception and evolution of attached partial cavitation. The experimental study is further enhanced by instantaneous wall-pressure measurements in cavitating flow.

2 Experimental Set-up

All the experiments were carried out in the Ecole Navale Cavitation Tunnel fitted with a 1m long and 0.192 m wide square cross test section. In this device, velocities of up to 15 m/s and pressures between 30 mbar and 3 bar can be achieved. The designed foil for this project is a 0.191 mm span two-dimensional cambered foil of the NACA66 series for which the theoretical coordinates are given in Astolfi *et al.* (2000). The relative maximum thickness τ is 12 % at 45% from the leading edge and the relative maximum camber is 2% at 50 % from the leading edge. The leading edge radius divided by the chord length is given by $\rho_{le}^{*} = 0.674\ \tau^{2}$. The theoretical lift coefficient at a given angle of incidence α is given by $C_l = 0.1092\ (1 - 0.83\ \tau)\ (\alpha + 2.35)$ for an inviscid unbounded flow (Valentine (1974)). The foil incidence was driven by a step by step DC motor. The distance between the trailing edge and the top of the test section was carefully adjusted at zero angle of incidence using a special gauge. The uncertainty on the angle of incidence was ±1/60 degrees. Two highly polished steel hydrofoils were manufactured. One had a 100 mm chord (denoted NACA66-12%-100 mm) and the second one had a 150 mm chord (denoted NACA66-12%-150 mm). The first one was used for detecting cavitation inception and cavitation development and has been the subject of previous studies (Astolfi *et al.* (2000)). The second one was specially fabricated for wall-pressure measurements and it was enlarged to be equipped with seventeen piezoresistive transducers. One accelerometer was also mounted in the foil but no result will be shown in the present paper.

Cavitation was visually observed under stroboscopic light. The inception condition was determined by increasing slowly the angle of incidence at a constant cavitation number until cavitation appeared. For sheet cavitation, the cavitation inception was determined until an organized spanwise cavitation pattern was visually detectable along a significant portion of the leading edge. This allowed us to eliminate local parasite cavitation events. This operation was repeated several times by different operators and the inception condition was a mean value of multiple readings. For bubble cavitation, the inception angle was determined until the first events of cavitating travelling bubbles were visually detected on the suction side. This allowed us to determine, $\alpha_i(\sigma)$, the angle of cavitation inception at a given cavitation number. It must be pointed out that the detection condition under visual observation corresponded to a limited cavitation (macroscopic detection) rather than a micro-scale cavitation detection, which should occur probably for smaller angles of incidence. The uncertainty of the measured cavitation inception numbers, in terms of the deviations from the mean values of repeated measurements is generally less than ± 0.04. The various patterns of cavitation were also determined depending on α and σ. This allowed us to determine the region for which partial cavitation occurred. In that case, the relative lengths *l/c* were also measured by photographing the foil surface using a Nikon digital camera put on the top of the test section.

Pressure measurements were carried out using piezo-resistive transducers (Keller AG 2 MI PAA100-075-010) of 10 bars maximum pressure. The pressure transducers were mounted into a small cavity with a 0.5 mm diameter pinhole (Figure 1.a). The resulting Helmoltz natural frequency of the cavity is about 85 kHz. in water. The first zero for a circular deflection transducer is theoretically $f_o = 1.76\ U/d$, where U is a typical convection velocity of the wall-pressure fluctuations and d the sensitive diameter (Lueptow (1993)). The frequency corresponds to the maximum frequency for which an attenuation of the pressure fluctuation spectrum, resulting from the spatial averaging over the transducer face, occurs theoretically. Here with d taken as the pinhole diameter and U taken as the nominal free stream velocity, f_o is 18.7 kHz (for U = 5.33 m/s). The transducer locations are given on Figure 1.b. As shown one set of ten transducers is aligned along the chord on the suction side from the leading edge (x/c = 0.05) up to the trailing edge (x/c = 0.9). Note that the suction side is referred to the most cambered surface of the foil. Two sets of three transducers were arranged parallel to this line to analyze eventual three - dimensional effects. One transducer was also mounted on the opposite face in order to control the effect on the pressure side of cavitation developing on the suction side.

The constructor sensitivity ranged between 50 and 100 mV/bar depending on the transducer, however an *in-situ* calibration was performed to take into account the transducer assembling. Before mounting the hydrofoil in the test section, the transducer cavities were water filled using a syringe. This was found to be very beneficial to degas the cavity. Running the tunnel under low-pressure level until no bubble was apparent on the pinhole of the cavity completed degassing of transducer cavities. The transducers were then calibrated all together by decreasing the pressure in the test section from 1.5 bars to 0.05 bar with a step of 0.05 bar at zero flow velocity. The transducer responses were found to be linear and the coefficients of the linear regression were used to convert Volts in pressure

units. To control any derive, the calibration procedure was performed systematically before and after one series of measurements. No attempt of a dynamic calibration was performed at the time being but will be the subject of future experiments.

The wall-pressure transducer signal were amplified, filtered and collected through a 16 channels, 16 bits A/D digitizer VXI HPE1432A at simultaneous sample with a maximum available sample frequency of 51.2 kHz. The control and the measurement storage was performed by a PC through an HPE8491A / IEE1394 PC link to VXI. The acquisition programs were developed *in-situ* and signal processing was developed using MATLAB® software. Two nominal sample frequencies have been selected. The first one at the maximum available frequency of 51.2 kHz and the second at a lower frequency of 1024 Hz corresponding to samples of 0.64 s and 4 s respectively. Spectral analysis was obtained from about the average of eight individual spectrums.

The nominal Reynolds number based on the foil chord length and the free stream velocity was 0.8 x 10^6. The value corresponded to a velocity of 8 m/s for the 100 mm foil and 5.33 m/s for the 150 mm foil. The nominal angle of incidence was 6 degrees.

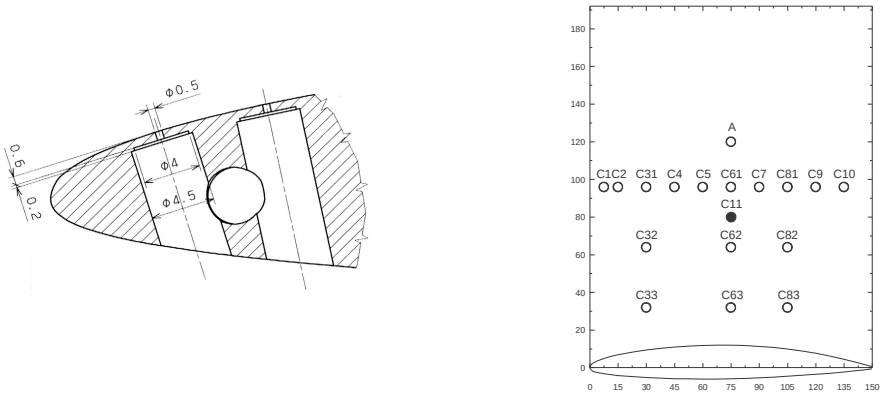

(a) (b)

Figure 1. a) Transducer cavity, b) Location of the pressure transducers, filled symbol is on the pressure side, *A* referees to the accelerometer, unit in millimeter.

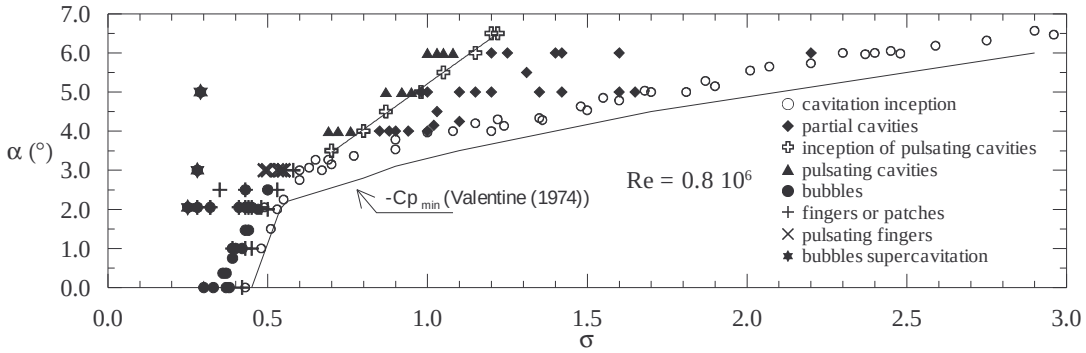

Figure 2. Cavitation inception and cavitation patterns, NACA66-12%-100 mm foil.

3 Results

Cavitation inception and cavitation patterns

Figure 2 summarizes the conditions for cavitation inception on the foil suction side. They were carefully determined for about fifty values of the cavitation number ranging between about 0.4 and 3. The abscissa denotes the cavitation number and the ordinate denotes the angle of incidence $\alpha_i(\sigma)$ for which cavitation was visually detectable. Also plotted are the theoretical (inviscid flow) values of the opposite of Cp_{min}. As shown, the cavitation inception experimental condition agrees well to the theoretical condition for incidence angles lower than about 2 degrees

(corresponding to bubble cavitation) but discards for larger values (corresponding to sheet cavitation). Although, viscous effect can explain this difference (Astolfi *et al.* (2000)), a bias due to the macroscopic detection of cavitation inception can not be neglected. Concerning cavitation development, several cavitation patterns are observed depending on the cavitation number and the angle of incidence as partial cavities, bubbles, patches or cavitation fingers. Partial cavities occur for angle larger than about 3° and σ larger than about 0.7. Bubble cavitation, cavitation fingers or patches are limited to a region corresponding to low cavitation numbers ($\sigma < 0.5$) and moderate angles of incidence lower than about 3°. Partial cavities of intermediate length (l^* lower than about 0.5) have a relatively stable behavior with weak variation of the cavity closure while shedding U-shaped vapor structures in the wake. As shown on Figure 3, the liquid - vapor interface has a glossy aspect over a short distance from the leading edge indicative of a laminar boundary layer developing on the interface. The extent of the laminar flow was found to be dependent on the velocity (Figures 3.b and 3.c for the same cavitation number but two velocities). Further away the interface becomes wavy and unstable over a large fraction of the cavity length. When the cavity becomes large, typically *l/c* larger than about 0.5, it exhibits a pulsating behavior while shedding larger vapor-filled structures. The transition is relatively well represented by the straight line shown on Figure 2. As the cavity closure region reached the foil trailing edge ($l^* \approx 1$) a typical behavior was observed with a periodic appearance and disappearance of the cavity at low frequency (of about few Hertz) inducing a strong fluid-structure interaction phenomenon. For stable cavity, the relative cavity lengths are plotted on Figure 4.a as a function of σ/α (α in degrees). As shown, in the early phases of development for σ/α lower than about 0.25, the cavity length increases slowly. In that case, the cavity appeared rather stable. By decreasing σ/α, the cavity then grew more rapidly until it reached about half the foil chord. At this stage the cavity closure strongly fluctuated. It was appeared interesting to look for scaling laws for cavity length development. It can be expected that for a given cavitation number, the cavity length depends on the difference between the angle of incidence and the angle of cavitation inception for which $l/c \approx 0$. This is shown on Figure 4.b where the cavity length is now plotted as a function of $\sigma/(\alpha - \alpha_i(\sigma))$ where $\alpha_i(\sigma)$ is deduced from Figure 3. Using such a scaling parameter it is found that *l/c* evolves as $[\sigma / (\alpha - \alpha_i(\sigma))]^m$ with an exponent *m* close to -2 *quasi*-independent on the test conditions.

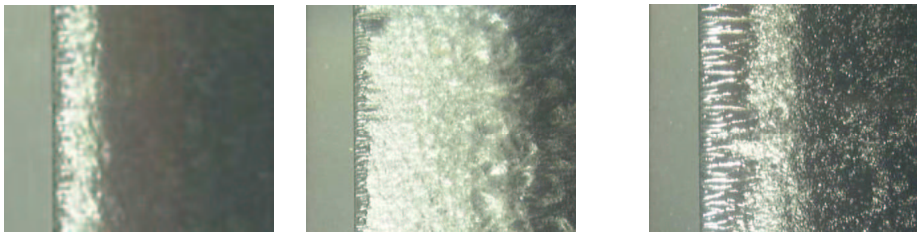

(a) (b) (c)

Figure 3. Photographs of leading edge partial sheet cavitation, NACA66-12%-100 mm foil, flow is from the left, α=6°, a) Re =0.8 10^6, σ =1.98, *l/ c*~0.045, b) Re =0.8 10^6, σ =1.31, *l/c*~0.325, c) Re =0.4 10^6, σ =1.30, *l/c*~0.205.

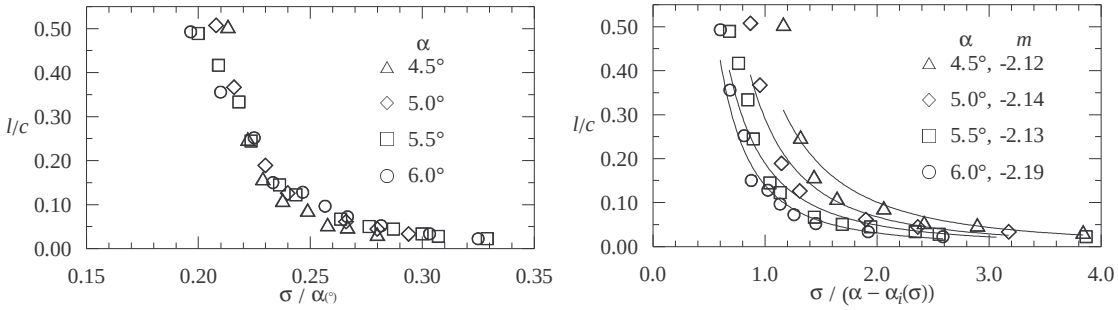

Figure 4. Cavity length, NACA66-12%-100 mm foil, a) as a function of σ/α, b) as a function of $\sigma/(\alpha - \alpha_i(\sigma))$. U = 5 m/s, Re = 0.8 10^6.

Pressure Measurements

The pressure coefficients are shown on Figure 5 for the non-cavitating flow and partial cavity flows developing on the suction side of the NACA66-12%-150 mm. On the figures, the isolated point corresponds to the transducer on the pressure side and the vertical bars are $\pm 1\ p_{rms}/(0.5\rho U^2)$ where p_{rms} is the root mean square of the pressure fluctuations. On Figure 5.a, the non-cavitating flow pressure coefficient exhibits a peak of -1.4 at x/c = 0.05. The peak is not the minimum pressure coefficient, which was found to occur closer to the leading edge by Astolfi *et al.* (2000) using velocity measurements and the Bernoulli hypothesis. When partial cavitation develops, the pressure coefficient is fairly constant and equal to the cavitation number in the cavity (Figure 5.b-d). At the end of the cavity, the pressure coefficient experiences an adverse pressure gradient and recovers the non-cavitating value downstream. The recompression is accompanied with a local increase of the pressure fluctuation intensity at the cavity closure. It can be noted that the pressure side is not affected by cavitation development on the suction side. As the cavity is larger than half the foil chord, it was shown that the cavity pulsated and that the cavity length varied periodically from the vicinity of the leading edge (x/c = 0.1) up to x/c = 0.7. This is observed on Figure 5.e which shows that the mean pressure coefficient up to x/c=0.5 is roughly an average value between the cavitation number (vapor) and the non-cavitating pressure coefficient (liquid). In that case, it can be also observed an increase of the pressure fluctuations all along the suction side. It can be also noted that the mean pressure coefficient on the pressure side is not affected. The pressure fluctuation intensity is clearly depicted on Figure 6.a for various cavity lengths including the pulsating cavity. As shown, a pressure peak is localized at the end of the cavity. For the pulsating cavity, the peak spreads out on the suction side.

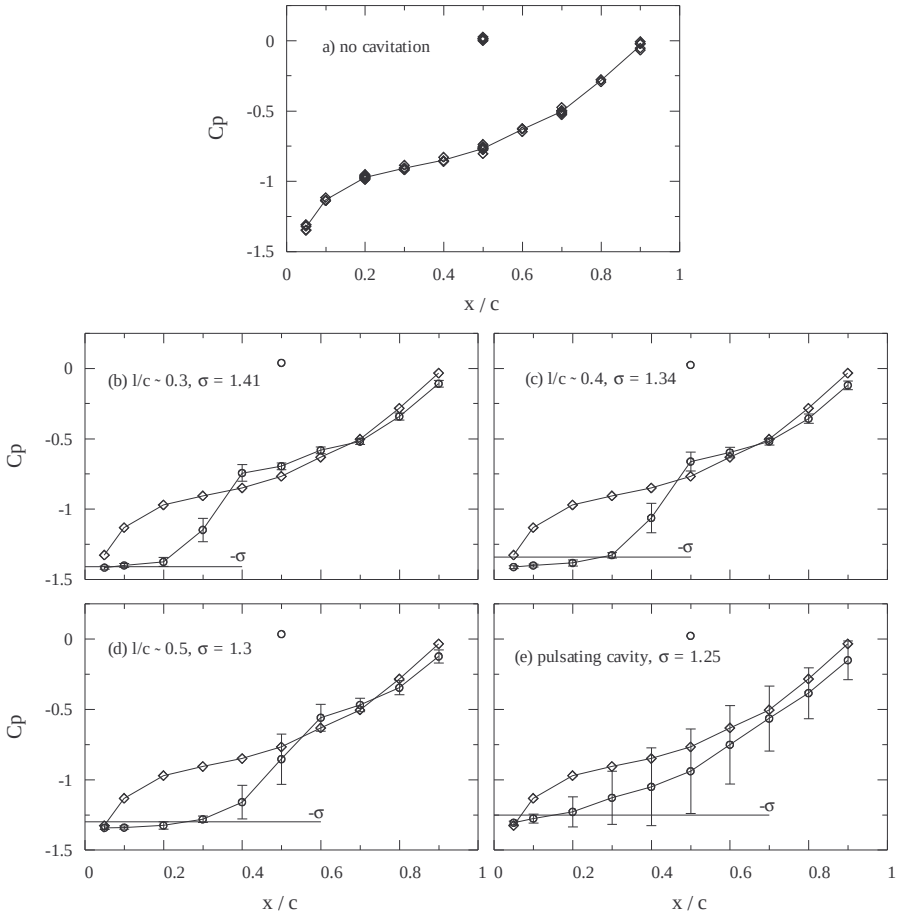

Figure 5. a) Non-cavitating pressure coefficient, the isolated data is on the pressure side, b) - d) Pressure coefficient for various cavity length e) Pulsating cavity. $\alpha = 6°$, Re = 0.8 10^6

Figure 6.b shows that the peak level increases as the cavitation number decreases (or the cavity expands) from about ten per cent up to thirty per cent of the dynamic pressure. Within the cavity ($x/c < l/c$), the pressure fluctuations are

fairly constant and close to the ones of the non-cavitating flow. An increase of the pressure fluctuations is recorded in the cavity wake. The spectral analysis on Figure 7 for *l/c* = 0.4 reveals that the increase of the pressure fluctuation intensity at the end of the cavity is associated to a frequency of 18.75 Hz (See Figure 7 for *x/c* = 0.4). As shown, this frequency still exists at *x/c = 0.5*. At *x/c* = 0.6, it spreads out and is not detected at *x/c* = 0.7. The corresponding instantaneous pressure coefficient in the closure region is shown on Figure 8 for x/c = 0.4 and x/c = 0.5. The frequency is also observed for others cavity lengths. As shown on Figure 9.a the frequency increases as the cavity length decreases. It is 14 Hz for *l/c* = 0.5 and 23 Hz for *l/c* = 0.3 corresponding to a Strouhal number based on the cavity length close to 0.2 in each case. For *l/c* = 0.5, two lower frequency peaks of 3.5 Hz and 7 Hz are also observed as shown on Figure 9.a. At this stage, a slight decrease of the cavitation number yielded to a pulsating cavity and the low frequency component at 3.5 Hz was amplified as shown on Figure 9.b. In that case, the cavity length experienced large changes, varying periodically from near *x/c* = 0.1 up to *x/c* = 0.7. This is clearly shown on Figure 10 where the instantaneous pressure coefficient passes from the cavitation number value (vapor) to the non-cavitating pressure coefficient (liquid). Figure 10 shows the existence of a time delay between two fronts detected on two transducers (see for instance x/c = 0.2 and x/c = 0.5). Furthermore, before recovering the non-cavitating condition, the pressure coefficient experiences a bump with high frequency components. As shown on Figure 10 a mean value of the bump is Cp = - 0.35 for x/c = 0.5. Both observations can be indicative of a reverse flow. A crude estimate of the reverse flow velocity can be computed from the time delay and the spacing between two transducers. A second way to estimate the reverse flow velocity is to assume that it can be deduced from the pressure coefficient using $U/U_\infty = (1\text{-}C_p)^{0.5}$. The first way gives 4 m/s and the second one gives a local velocity of 6.18 m/s with Cp = - 0.35. Both values are of the order of the free stream velocity.

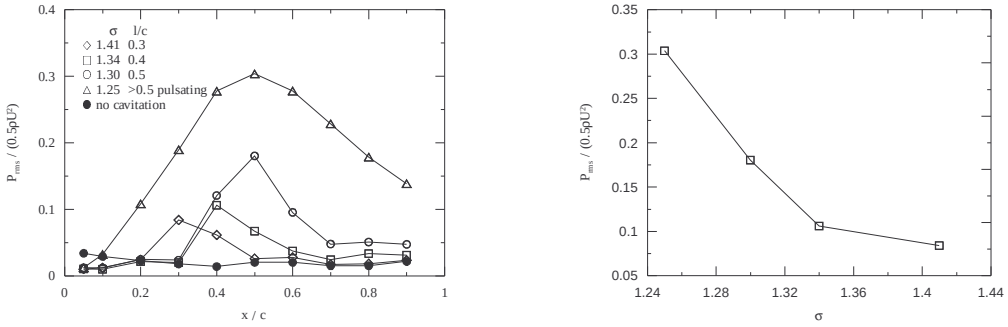

Figure 6. a) Pressure fluctuation intensity, b) Relative maximum of p_{rms} as a function of σ. α = 6°, Re=0.8 10^6.

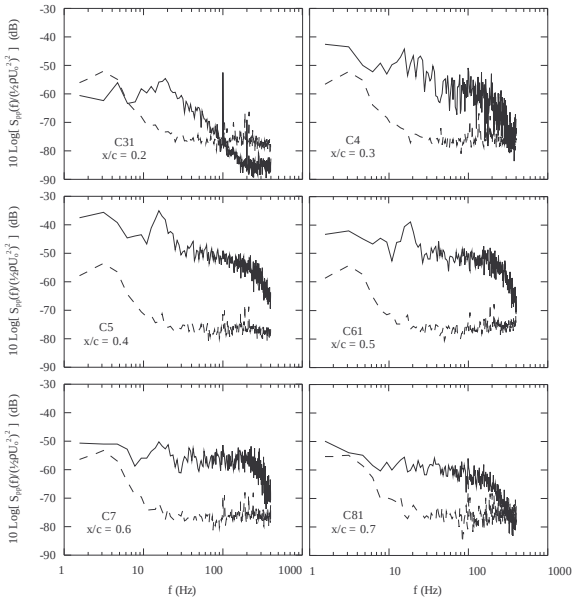

Figure 7. Power spectral density, dashed line is the non-cavitating flow. α = 6°, Re = 0.8 10^6, σ = 1.34, *l/c* ~ 0.4

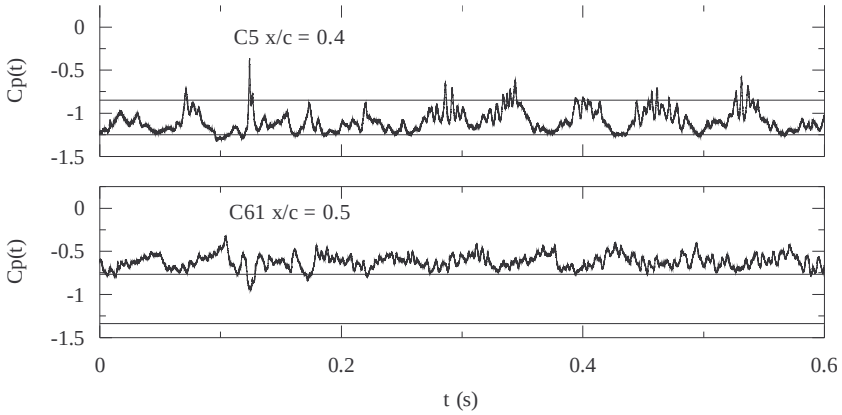

Figure 8. Instantaneous pressure coefficient. The solid horizontal lines are the cavitation number and the non-cavitating pressure coefficient. $\alpha = 6°$, $\sigma = 1.34$, $l/c \sim 0.4$, Re = 0.8 10^6.

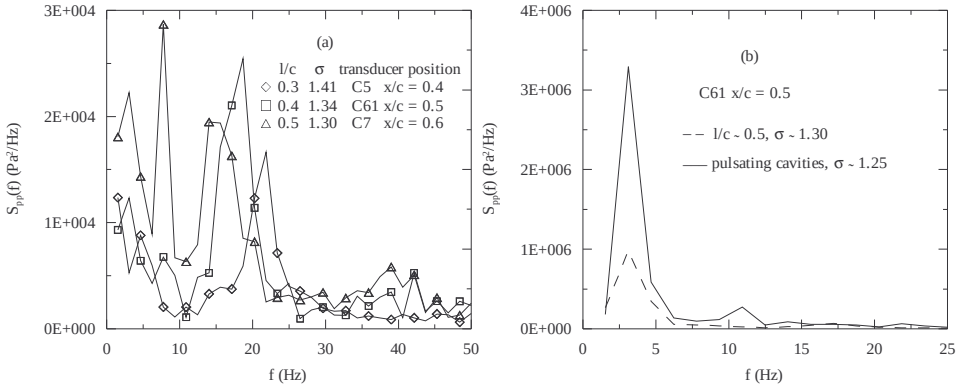

Figure 9. Pressure power spectral density. $\alpha = 6°$, Re = 0.8 10^6.

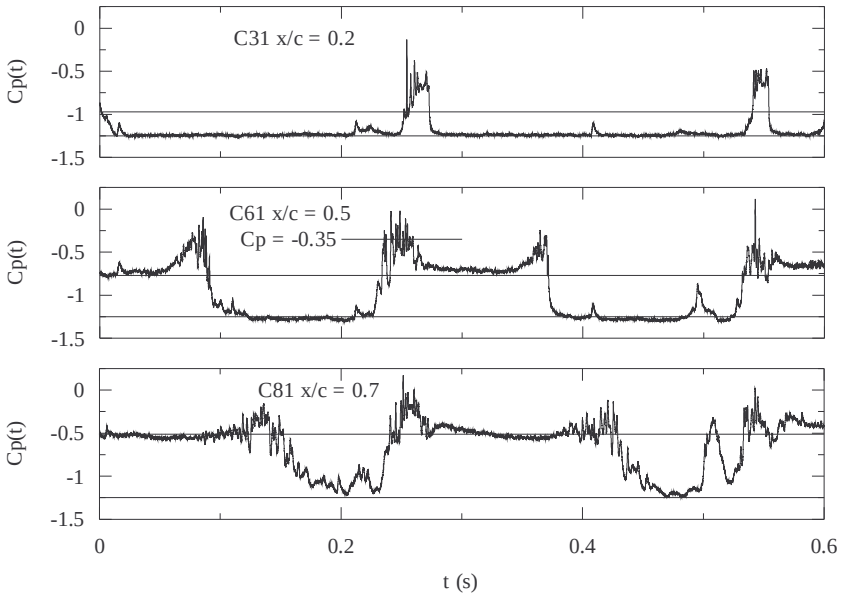

Figure 10. Instantaneous pressure coefficient during pulsating cavity, the horizontal lines indicate the operating cavitation number and the non-cavitating pressure coefficient. $\alpha = 6°$, $\sigma = 1.25$, Re=0.8 x 10^6.

4 Conclusion

An investigation of partial leading edge cavitation was carried out including cavitation inception conditions, cavitation patterns together with cavity lengths measurements and wall-pressure measurements. For cavities that did not exceed half the foil chord, it was shown that the pressure was very close to the liquid vapor pressure in the cavity and that it recovered the non-cavitating flow value outside. At the closure of the cavity, the pressure fluctuation intensity increased significantly. The spectral analysis revealed a Strouhal number, based on the cavity length, close to 0.2. As the cavity length grew and was larger than about half the chord length, the cavity exhibited a pulsating behavior with large change in cavity length at a lower frequency. The case of a reverse flow is analyzed.

Acknowledgments

The authors wish to express their deep appreciation for the continuous support of R. Saget and M.P. J. Gentrau and of the support of the Ecole navale, Ministry of Defense, France. Special thanks to C. Griffin for partial proofreading.

References

ARNDT, R.E.A., SONG, C.C.S., M. KJELDSEN, HE J., & KELLER A., 2000 Instability of partial cavitation: a numerical/experimental approach," PROCEEDINGS OF 23RD SYMPOSIUM ON NAVAL HYDRODYNAMICS, 5-9, 2000, ROUEN, FRANCE.

ASTOLFI J-A, LEROUX J.-B., DORANGE P., BILLARD J.-Y., DENISET F., DE LA FUENTE S., 2000, An experimental investigation of cavitation inception and development on a two dimensional hydrofoil. *J. Ship Res*. 44, No 4, Dec. 2000, 259-269.

ARAKERI, V. H 1975 Viscous effects on the position of cavitation separation from smooth bodies. *J. Fluid. Mech* **68**, part 4, 779-799.

BRIANÇON-MARJOLLET L., FRANC J.-P. and MICHEL J.-M. 1990 Transient bubbles interacting with an attached cavity and boundary layer. *J. Fluid. Mech* **218**, 355-376.

BREWER, W. H. & KINNAS, S. A. 1995 Experimental and computational investigation of sheet cavitation on a hydrofoil. The 2nd Joint ASME/JSME Fluids Engineering Conference On Laser Anemometry, August 12-13, Hilton Head Island, South Carolina .

CALLENAERE, M., FRANC, J.P. & MICHEL, J.M. 1998 Influence of Cavity Thickness and Pressure Gradient on the Unsteady Behavior of Partial Cavities. Third International Symposium on Cavitation, April 7-10, Grenoble, France

FRANC, J.-P., & MICHEL, J.-M. 1985 "Attached Cavitation and the Boundary Layer : Experimental Investigation and Numerical Treatment", *J. Fluid. Mech*. **154**, 63-90.

HUANG, T. T. 1986 The effect of turbulence stimulators on cavitation inception of axisymetric headforms. *J. Fluids Engng* **108**, 261-268.

HUANG, T. T., & PETERSON, F. B. 1976 Influence of viscous effects on model/full-scale cavitation scaling, *Journal of Ship Research*, **20**, N°4, 215-223.

KAWANAMI, Y., KATO, H., & YAMAGUCHI, H. 1998 Three-dimensional characteristics of the cavities formed on a two-dimensional hydrofoil", Third International Symposium on Cavitation, April 7-10, Grenoble, France.

KINNAS, S.A., and FINE, N.E. 1993 A Numerical nonlinear analysis of the flow around two and three-dimensional partially cavitating hydrofoils. *J. Fluid. Mech*, **254**, 151-181.

KUBOTA, A., KATO, H., and YAMAGUCHI, H 1992 "A New Modeling of Cavitating Flows: a Numerical Study of Unsteady Cavitation on a Hydrofoil Section", *J. Fluid. Mech.*, **240**, 59-96.

LABERTEAUX , K R., & CECCIO, S. L. 2001 Partial cavity flows. Part 1. Cavities forming on models without spanwise variation *J. Fluid. Mech*, **431**, 1-41.

LE, Q., FRANC, J.-P., & MICHEL, J.-M. 1993 "Partial cavities: pressure pulse distribution around cavity", *J. Fluids Engng*, Vol. 115, pp. 249-254.

LI, C.-H., & CECCIO, S. L. 1996 Interaction of single travelling bubbles with the boundary layer and attached cavitation, *J. Fluid. Mech.* **322**, 329-353.

LUEPTOW, R.M, 1993, "Wall Pressure Transducer Spatial Resolution", NCA- Vol. 15. 168, Flow Noise Modeling, Measurement, and Control, ASME 1993, 49-55.

PELLONE C., MAÎTRE T., & BRIANÇON-MARJOLLET L. 2000 Partially cavitation hydrofoils: experimental and nulerical analysis, *J. Ship Res*, **44**, N°1, 40-58.

VALENTINE, D.T. 1974 "The effect of Nose Radius on the Cavitation Inception Characteristics of Two-Dimensional Hydrofoils", Report 3813 of the *Naval Ship Research and Development Center*, Bethesda, Maryland 20034.

ZHANG, Y., GOPALAN, S., & KATZ , J. 1998 On the flow structure and turbulence in the closure Region of attached cavitation. In *22nd Symposium on Naval Hydrodynamics*, August, Washington D.C., 227-238.